PREDICTION OF FORMABILITY OF BI-AXIAL PRE-STRAINED DUAL PHASE STEEL SHEETS USING STRESS BASED FORMING LIMIT DIAGRAM

Shamik Basak[1], Kaushik Bandyopadhyay [2], Sushanta Kumar Panda[3*], Partha Saha[4]

Indian Institute of Technology Kharagpur, Kharagpur, 721302,
[1] shamikmech@gmail.com
[2] kaushik.me08@gmail.com
[*3] sushanta.panda@mech.iitkgp.ernet.in
[4] psaha@mech.iitkgp.ernet.in

Abstract

Dual phase (DP) steel is of great interest for automotive part manufacturers due to its excellent combinations of strength and formability. Complex components involving three-dimensional stampings are usually fabricated through multistage sheet forming operations. The ability of a sheet metal to be deformed into a specific desired shape by distributing strain over arbitrary tool surface depends on complex interaction of material, process and design variables. The strain based forming limit diagram (ε-FLD) is often used as a measure of formability in the press shop due to convenience of measuring the limiting strain. However, it was reported by previous researchers that the ε-FLD of sheet metal shifts after pre-strain due to the initial forming operations. Hence, this present work proposes a mathematical framework for constructing σ-FLD of different pre-strained sheet incorporating Barlat-89 yield criterion with different hardening laws. The formability of biaxially pre-strained DP600 was evaluated experimentally in two stages. The forming behaviour of pre-strained material was predicted by finite element model using the σ-FLD, and prediction results matched very closely with experimental data. It was also observed that the σ-FLD was robust and underwent insignificant changes due to the change in the pre-strain path.

Keywords: Stress based forming limit diagram, DP600, Pre-strain, LS-DYNA

1. Introduction

Recently automotive industries are interested in use of various advanced high strength steels (AHSSs) to fabricate light weight components with improved vehicle performances. Among the AHSS family of steels, the dual-phase (DP) steels are the most favourite to the manufacturing industries due to their inherent combinations of high strength and ductility. However, an accurate prediction of the formability is extremely important for DP steels before applications in automotive parts. Formability is a measure of the amount of deformation a sheet metal can withstand prior to localize thinning which ultimately leads to tearing or splitting. Forming Limit Diagram (FLD) is one of the prevailing measures of formability. It represents the forming limit surface strains that the sheet can withstand before failure (necking/splitting) in terms of major (ε_1) and minor (ε_2) principal strains. This strain based FLD (ε-FLD) is used as the diagnostic tool for failure in sheet metal forming industries, and hence, frequently used as damage model in finite element modelling (FEM). This diagram was first brought into sheet forming industries by Keeler and Bakofen (Keeler and Bekofen,1963) and Goodwin (Goodwin,1968). Many researchers showed experimentally that the shape and position of ε-FLD shifts depending on the amount and the type of pre-strain.

This dynamic nature of ε-FLD was confirmed by extensive experiment done by Graph and Hosford. (Graph and Hosford,1993). They reported that forming limit decreases with bi-axial prestrain, and simultaneously shifts more towards the tension-tension side for Al 2008 T4. On the contrary, the limiting strain increases both with uniaxial and plane strain pre-strain for the same material, and shifts as shown in Figure 1(a). This signifies the sensitivity of ε-FLD on strain path, and hence, its use in complex sheet forming processes with non-proportional strain path is no more valid. It is very difficult to trace the dynamic nature of ε-FLD shift after each stage in a multi-stage forming process. The most capable solution for dealing the above issue is the use of stress-based FLD (σ-FLD) curve. Stoughton (Stoughton,2000) had converted the ε-FLD reported by Graph and Hosford (Graph and Hosford,1993) to σ-FLD, and concluded that σ-FLD is not affected by change of the strain path. More recently Yoshida (Yoshida et al.,2007) concluded that if the material was described by isotropic hardening model, the σ-FLDs were path-independent.

However, the change in formability in multi-stage forming process of DP steel was not reported in openly available literatures. Hence, the main goal of the present work is to experimentally design a two-stage stretch forming set up to evaluate the forming

behaviour of different biaxial pre-strained DP steel. The σ-FLD was evaluated theoretically incorporating Barlat-89 anisotropic yield criterion with different hardening laws. Finally, the developed σ-FLD was implemented in the FEM to predict the forming behaviour of pre-strained materials, and the results were validated with experimental results.

2. Theoretical background

The limiting strain in FLDs of sheet metals usually evaluated through sheet forming a series of circular grid marked samples of different widths by hemispherical punch and dies with drawbead. The details are available in literature (K.Nakazima et al.,1968). However, the principle stress components of a deformed sheet metal are represented in σ-FLD, instead of strain components. The important components which are required to depict the plastic behaviour of a material in a general stress state are: (a) yield criterion expressing a relationship between the stress components at the moment when plastic yielding occurs, (b) associated flow rule describing the manner in which plastic strain depends upon a given stress state, and (c) hardening rule describing the evolution of the yield stress during forming process.

2.1 Barlat-89 yield criterion

Barlat (Barlat and Lian,1989) proposed a yield criterion in the form of:

$$f = a|k_1 + k_2|^M + a|k_1 - k_2|^M + c|2k_2|^M = 2\bar{\sigma}^M \quad (1)$$

Where a, c, h & p are material anisotropy constant related to r_0 and r_{90} (the anisotropy coefficient in rolling direction and transverse direction respectively). M is chosen according to the crystallographic structure of the material. Here k_1 and k_2 are invariants of the stress tensor and they are defined as,

$$k_1 = \frac{\sigma_x + h\,\sigma_y}{2};\ k_2 = \sqrt{[(\frac{\sigma_x - h\,\sigma_y}{2})^2 + p^2\sigma_{xy}{}^2]}$$

$$a = 2 - c = 2 - 2\sqrt{\frac{r_0}{1+r_0}\frac{r_{90}}{1+r_{90}}},\ h = \sqrt{\frac{r_0}{1+r_0}\frac{1+r_{90}}{r_{90}}}$$

Now, $p\sigma_{xy}=0$ for anisotropic thin rolled sheet. Hence the parameters boil down to:

$$k_1 + k_2 = \sigma_x \qquad k_1 - k_2 = h.\sigma_y$$

As stress tensor coincides with the principal anisotropic axis, the yield criterion can be expressed in terms of principal stresses as below for plane stress condition($\sigma_3 = 0$).

$$f = a|\sigma_1|^M + a|h\sigma_2|^M + c|\sigma_1 - h\sigma_2|^M = 2\bar{\sigma}^M \quad (2)$$

Plastic strain increment is governed by flow rule:

$$d\varepsilon_{ij} = d\lambda\frac{\partial f(\sigma_{ij})}{\partial\sigma_{ij}}$$, where dλ = non-negative constant

Applying flow rule in equation 2 and upon simplification the equation can be written in the form of stress ratio as:

$$\xi = \frac{\bar{\sigma}}{\sigma_1} = [\frac{1}{2}\{a + a|h\alpha|^M + c|1 - h\alpha|^M\}]^{\frac{1}{M}} \quad (3)$$

,where $\alpha = \frac{\sigma_2}{\sigma_1}$

Here ξ is defines as the ratio of the effective stress (which can be calculated by the hardening laws) and major stress. Again strain ratio $\rho = \frac{d\varepsilon_2}{d\varepsilon_1}$ can be written in the form of α as:

$$\rho = \frac{a|h\alpha|^{M-1} - ch|1 - h\alpha|^{M-1}}{a + c|1 - h\alpha|^{M-1}} \quad (4)$$

The effective strain is expressed from the definition of plastic work as follows:

$$\bar{\varepsilon} = \frac{\varepsilon_1}{\xi}(1 + \rho\alpha) \quad (5)$$

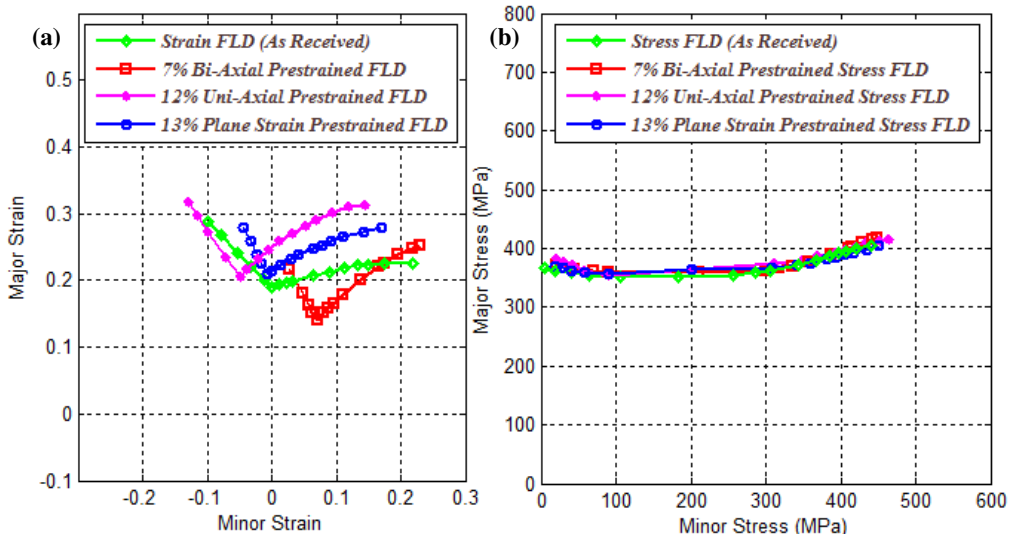

Figure 1 Conversion to σ-FLD for different pre-strain condition(a)ε-FLD[Graph and Hosford,1993**](b)σ-FLD**

Table 1 Uniaxial tensile properties of DP600 steel used in the present study

Grades and gauges	Yield strength (MPa)	Ultimate tensile strength (MPa)	% Total elongation	Anisotropic properties		
				r_0	r_{45}	r_{90}
DP600 (1.2)	407	665	19.12	0.96	0.93	1.05

Table 2 Material constants evaluated incorporating different hardening models

Hollomon law			Swift law				Modified Voce law				
K (MPa)	n	R^{2*}	ε_0	K (MPa)	n	R^{2*}	A	B_0	B_1	C	R^{2*}
1125	0.21	0.9836	0.005	1140	0.20	0.9980	839	361	202	10	0.9843

*Here, R^2 is defined as the *coefficient of determination* which indicates how well data points fit a line or curve

2.2 Hardening laws

Strain hardening is the strengthening of a metal by plastic deformation, and three hardening laws are considered in this work, namely Hollomon, Swift and modified Voce model.

The Hollomon equation is given by

$$\bar{\sigma} = K.\bar{\varepsilon}_P^{\,n} \tag{6}$$

where $\bar{\sigma}$ and $\bar{\varepsilon}_P$ are respectively the effective stress and plastic strain. K (known as strength coefficient) and n (known as stain hardening exponent) are material constants.

The Swift equation is given by

$$\bar{\sigma} = K.(\varepsilon_0 + \bar{\varepsilon}_P)^n \tag{7}$$

The parameters K, n and ε_0 are material constants.

Modified Voce equation is given by

$$\bar{\sigma} = A - B_0.e^{(-C.\bar{\varepsilon}_P)} + B_1.\bar{\varepsilon}_P \tag{8}$$

where A, B_0, B_1 and C are the material constants. All these material constants can be calculated by fitting the experimentally determined true stress- true strain diagram.

3. Construction and validation of stress based forming limit diagram

The major and minor strain value after prestrain is defined by ε_{1i} and ε_{2i} respectively, and that of after Step II is defined by ε_{1f} and ε_{2f} respectively. Amount of effective strain induced in the specimen during pre-strain can be calculated from the equation 5 by calculating the ratio like ρ, α and ξ as formulated by the equation 3 and 4. Similarly for step II, effective strain has been calculated. Finally the effective stress at the end of the secondary stage was calculated by hardening laws by following the relation:

$$\bar{\sigma} = f\{\bar{\varepsilon}\ (\varepsilon_{1i}, \varepsilon_{2i}) + \bar{\varepsilon}\ (\varepsilon_{1f} - \varepsilon_{1i}, \varepsilon_{2f} - \varepsilon_{2i})\} \tag{9}$$

From this relation, principal stresses were calculated with the ratio ξ and α. These major and minor principal stress values were mapped in stress

locus to obtain σ-FLD.

For validation of σ-FLD, the ε-FLD data of as received and different pre-strain condition has been collected from literature (Graf and Hosford, 1993) for material Al 2008 T4 (Figure 1(a)). All the ε-FLDs were converted to σ-FLD incorporating Barlat-89 anisotropic yield criterion coupled with Hollomon hardening law. The final σ-FLDs are shown for all pre-strain condition in Figure 1(b), and it can be seen that all the scattered pre-strain ε-FLD curves merged into a single line. From Figure 1(b), the insensitivity of σ-FLD on strain path has been verified.

4. Experimental procedure

4.1 Material selection

The commercial grade dual phase steel of a particular type namely DP600 with a thickness of 1.2 mm was investigated in the present study. The various properties, like ultimate tensile strength, 0.2% offset yield strength, uniform elongation, total elongation, r-value (plastic strain ratio) were evaluated and reported in Table 1. The true stress – true strain data from uniaxial tensile test of DP600 was fitted and extrapolated with the Hollomon, Swift and Voce hardening laws and the different coefficient values for different hardening laws are determined by best fitting curves. The different coefficient values were tabulated in Table 2.

4.2 Multi stage forming experiment

Complex strain paths were induced in the sheet metal using combinations of two linear strain paths. The biaxial pre-strain has been induced to the sheet metal in the step-I, and out-of-plane stretch forming operation has been carried out to determine formability in step-II. The details are mentioned below.

STEP- I: To induce pre-strain into the specimen

To conduct this test, an in-plane stretch forming set up (Figure 2) was conceptualized, designed and fabricated. The sheet metal together with brass washer (Figure 2) was together kept over the die. Thick film of lubrication was provided between the punch and the washer before the flat punch deformed the test specimen. As the punch moved down, the hole in the washer expands in radial direction inducing radial friction forces in the contact region between the test piece and washer. This friction prevents the test piece from getting fractured near the punch corner. Circular grids of 2.5 mm diameter were marked on the blanks by electrochemical etching technique to measure major and minor strains in the specimen after deformation.

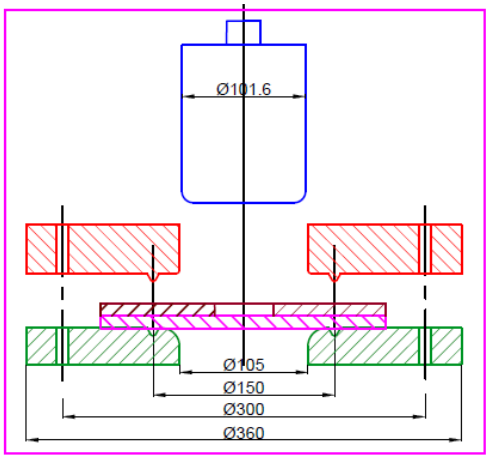

Figure 2 Set-up for biaxial pre-strain (Step- I)

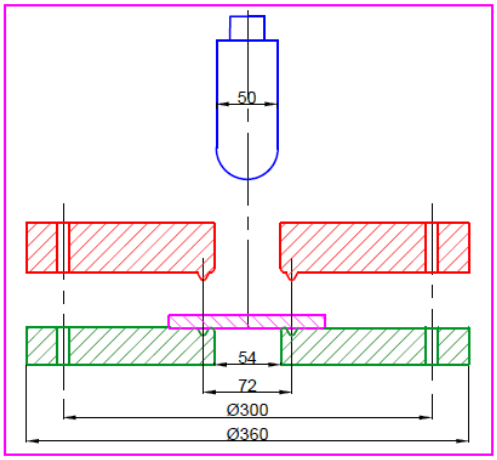

Figure 3 Out-of-plane stretch forming (Step- II)

STEP- II: Stretch forming operation on pre-strained specimen

After measuring the pre-strain, the bottom portion was trimmed by wire EDM. This resultant blank was treated as input test piece for Step II. The formability of the pre-strained blank was evaluated in terms of limiting dome height by stretch forming using a hemispherical die punch set up as shown in Figure 3. The experiments were stopped when a visible neck or initiation of fracture were observed on the specimens.

5. Finite element analysis

FE simulations of the both the forming steps were carried out using LS-DYNA 971. All tooling surfaces such as the die, punch and blank holder (or binder) were modelled as rigid bodies. The coefficient of friction between the punch and blank was 0.01 in first step (as thick film lubrication was applied) and 0.15 in second step. However, the coefficient of friction

between the blank and die was 0.15 in both the steps. The Barlat-89 non-quadratic yield criterion was used in modelling the deformable blank. The predicted major and minor strain data points at each step of the deformation in the FE simulation were interposed into the ε-FLD. In this work, the experimental ε-FLD for DP600 with 1.2 mm sheet thickness was taken from literature (Kilfoil,2007). Corresponding stress values in both principal directions were also evaluated and then plotted on σ-FLD. The time step in which the strain or stress value reached to the limiting value was referred to predict failure.

6. Results and discussion

6.1 Dome height prediction

The limiting dome height predicted by ε-FLD and σ-FLD is equal, and comparable with that of experimental result for as received material. Whereas, in case of pre-strained conditions, the result predicted by σ-FLD is closer to the experimental result compare to the results predicted by ε-FLD (Table 3). This fact can be well explained through the nature of shifting of ε-FLD curve for pre-strained condition. In case of parent material (DP600) nearly bi-axial strain path had been observed during pre-straining. It was reported that the ε-FLD shifted downward by lowering the limiting strain, and this resulted smaller dome height.

Table 3 Comparison of limiting dome height of DP600 at different pre-strain condition

Material	Experimental data		Predicted data (by LS DYNA)		
	% of pre-strain	Final dome height (mm)	% of pre-strain	Final dome height (mm)	
				using ε-FLD	using σ-FLD
DP600	As received	16.55	As received	17.18	17.18
	6.3%	13.67	6.2%	14.82	13.35
	10.9%	12.27	11.0%	14.02	11.82

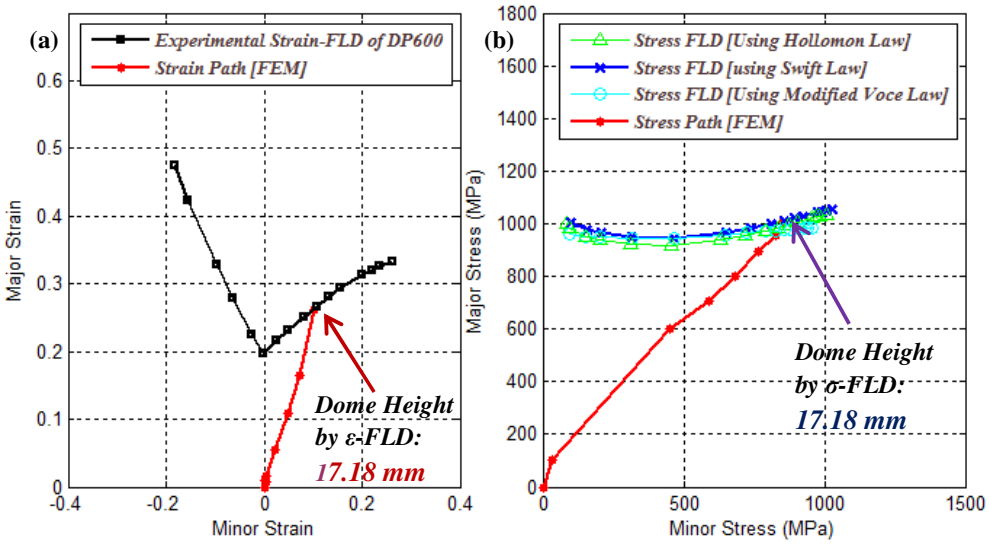

Figure 4 (a) Strain and (b) stress path during forming of DP600 as received material

6.2 Strain and stress path during different steps

It can be further observed form Figure 4 that Swift hardening law is predicting better forming limit in comparison with that of Hollomon and modified Voce hardening laws. In Figure 5, stain and stress path has shown for 6.3% pre-strain condition for DP600. Also from the Figure 5, it can be noticed that the slope of the strain path changes from first step to second step in ε-FLD. In the first step the strain path is more towards biaxial side compared to second step. This is because a thick film of lubrication was applied which reduced the friction in the first step, and helped to achieve nearly bi-axial pre-strain. On contrary, the second step stretch forming operation was performed in completely dry condition. It can be observed that the actual failure takes place far before the time step when ε-FLD predicts failure. The σ-FLD is able to predict the correct time step when the failure occurs. It is clear from these plots that ε-FLD is unable to predict formability in the present multistage forming process. However, the σ-FLD is insensitive to the deformation history, and hence it is suitable for complex forming process.

6.3 Validation of load progression and thickness distribution

The load-displacement curves were obtained through data acquisition system, and it was observed that the load requirement for deformation increased with the increase in punch travel. Similar trend was also predicted from FE simulation as shown in Figure 6. The thickness variation was measured and plotted as shown in Figure 7. Negligible thinning was observed at the pole due to high friction between punch and blank. However the maximum thinning

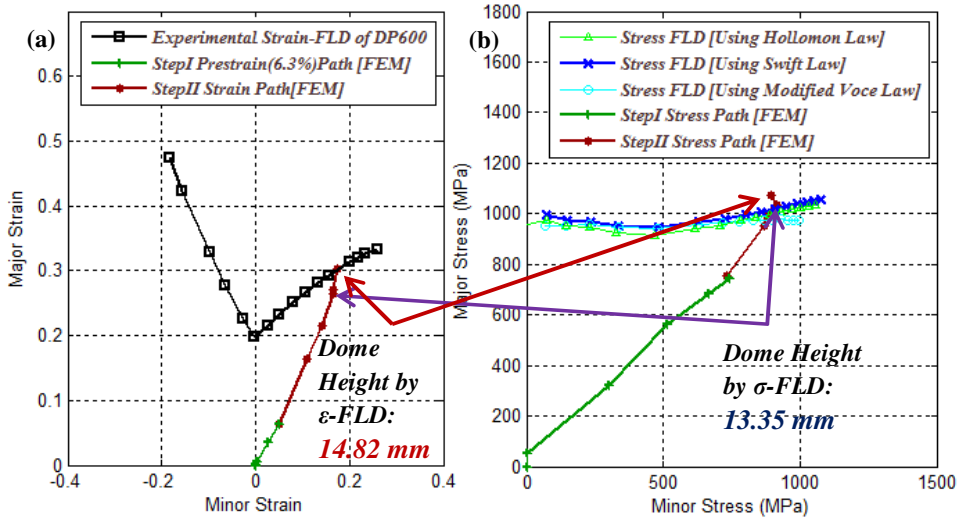

Figure 5 (a) Strain and (b) stress path during forming of 6.3% pre-strained DP600 material

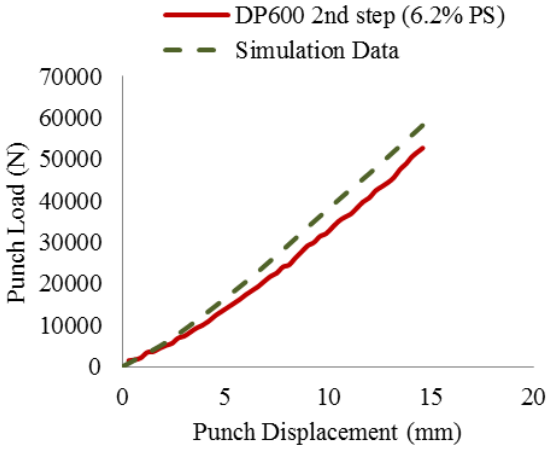

Figure 6 Load-displacement curve during deformation of 6.3% pre-strained DP600 metal

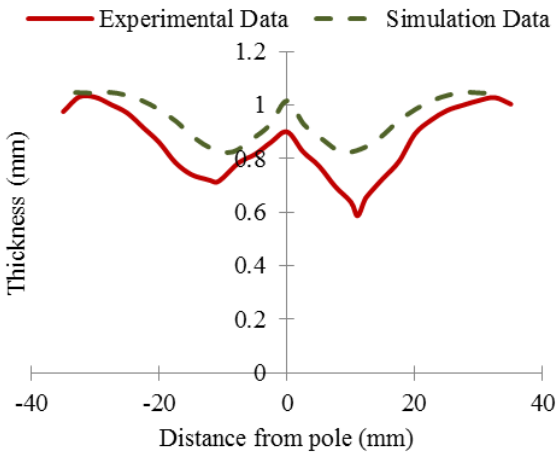

Figure 7 Thickness distribution in a stretch formed cup from 6.3% pre-strained DP600 metal

was observed at the location where punch was starting to be out of contact from the blank at a certain distance from the pole.

7. Conclusions

The followings are the major conclusions.

I. A serious restriction of ε-FLD is that it applies only for proportional loading condition. The σ-FLD was evaluated successfully for different pre-strain conditions using ε-FLD by Barlat-89 yield criterion and different hardening models. It was observed that σ-FLD is insensitive to the deformation history, and depends only on stress state.

II. Limiting dome height predicted by FE simulation incorporating ε-FLD is more as compared to σ-FLD for bi-axially pre-strained DP600 specimens.

III. Barlat-89 yield criterion coupled with Swift hardening law predicts formability of pre-strain

DP600 closely to the experimental limiting dome height, thickness distribution and load progression results.

References

Arrieux, R., Bedrin, C., and Boivin, M. (1982, May), Determination of an intrinsic forming limit stress diagram for isotropic metal sheets. In *Proceedings of the 12th Biennial Congress of the IDDRG* (pp. 61-71).

Barlat, F., and Lian, J. (1989), Plastic behavior and stretchability of sheet metals. Part I: A yield function for orthotropic sheets under plane stress conditions. *International Journal of Plasticity*, 5(1), 51-66.

Graf, A. F., and Hosford, W. F. (1993), Calculations of forming limit diagram for changing strain paths. *Metallurgical Transactions* A, 24(11), 2497-2501.

Goodwin, G. M. (1968), Application of strain analysis to sheet metal forming problems in the press shop (No. 680093). *SAE Technical Paper*.

Keeler, S. P., and Backofen, W. A. (1963), Plastic instability and fracture in sheets stretched over rigid punches. *ASM TRANS* Q, 56(1), 25-48.

Kilfoil, L. J. (2007), In-plane plane strain testing to evaluate formability of sheet steels used in tubular products. MS Thesis, Queen's University, Ontario, Canada, Chap. 2, p. 33

Kleemola, H. J., and Pelkkikangas, M. T. (1977), Effect of predeformation and strain path on the forming limits of steel, copper and brass. *Sheet Metal Industries*, 64(6), 559-592.

Matsuoka, T., and Sudo, C. (1969), Effect of strain path on the fracture strain of steel sheet. *Sumitomo Search, May 1969*,--1--, 71-80.

Panda, S. K., Hernandez, V. B., Kuntz, M. L., and Zhou, Y. (2009), Formability analysis of diode-laser-welded tailored blanks of advanced high-strength steel sheets. *Metallurgical and Materials Transactions* A, 40(8), 1955-1967.

Raghavan, K. S. (1995), A simple technique to generate in-plane forming limit curves and selected applications. *Metallurgical and Materials Transactions* A, 26(8), 2075-2084.

Stoughton, T. B. (2000), A general forming limit criterion for sheet metal forming. *International Journal of Mechanical Sciences*, 42(1), 1-27.

Stoughton, T. B. (2001), Stress-based forming limits in sheet-metal forming. *Journal of Engineering Materials and Technology*, 123(4), 417-422.

Stoughton, T. B., and Yoon, J. W. (2012), Path independent forming limits in strain and stress spaces. *International Journal of Solids and Structures*, 49(25), 3616-3625.

Yoshida, K., Kunwabara, T., and Kuroda, M. (2007), Path-dependence of the forming limit stresses in a sheet metal. *International Journal of Plasticity*, 23(3), 361-384.